Eur. J. Mech. B - Fluids 19 (2000) 213–227

S0997-7546(00)00108-4/FLA

Convection in a low Prandtl number fluid layer rotating about a vertical axis

Richard M. Clever [a,*], Friedrich H. Busse [b,1]

[a] *Institute of Geophysics and Planetary Physics, University of California at Los Angeles, USA*
[b] *Institute of Physics, University of Bayreuth, 95440 Bayreuth, Germany*

(Received 31 March 1999; revised 11 October 1999; accepted 28 October 1999)

Abstract – Two- and three-dimensional convection flows in a horizontal layer of a low Prandtl number fluid heated from below and rotating about a vertical axis are studied numerically with a Galerkin method. Solutions for subcritical steady finite amplitude convection and convection in the form of standing oscillations are obtained. Parameter regimes that appear to be attainable in laboratory experiments have been emphasized. The stability of subcritical two-dimensional steady convection has been investigated and three-dimensional chaotic states of convection have been found. © 2000 Éditions scientifiques et médicales Elsevier SAS

Galerkin method / low Prandtl number fluid / rotating convection

1. Introduction

Thermal convection in a fluid layer heated from below and rotating about a vertical axis has received much attention in recent years because of its unusual dynamical properties. Contrary to the usually stabilizing influence of side walls it was found that convection in the form of a drifting mode attached to a side wall sets in at Rayleigh numbers much below the critical value for the onset of convection in the bulk of the fluid layer (Goldstein et al. [1]; Herrmann and Busse [2]; Kuo and Cross [3]). The spatio-temporal chaos induced by the Küppers–Lortz instability continues to receive much attention and numerous experimental studies (see, for example, Busse and Heikes [4]; Zhong et al. [5]; Hu et al. [6]) and numerical simulations (Tu and Cross [7]; Millán-Rodriguez et al. [8]; Pesch [9]; Julien et al. [10]) have been carried out.

Since convection can be visualized most easily in fluids with Prandtl numbers of the order unity or larger, research has focused on this range of Prandtl numbers P. But theory suggests that even more unusual dynamical phenomena can be expected in fluids of low Prandtl numbers. It is well known from the early work of Chandrasekhar [11] that the onset of convection occurs in the form of oscillations when the Prandtl number is below $P = 0.6766$, provided the rotation rate is sufficiently high. This value of P is independent of the boundary conditions for the velocity field since these do not influence the onset of convection in the limit of high rotation rates (Clune and Knobloch [12]). Approximately within the same range of Prandtl numbers where linear theory predicts the onset in the form of oscillatory modes, the bifurcation of steady modes of convection becomes subcritical according to nonlinear theories (Veronis [13,14]; Clever and Busse [15]; Clune and Knobloch [12]). Not much is known, however, about the finite amplitude properties of oscillatory convection and about the three-dimensional flows that replace the unstable subcritically bifurcating solutions in the form of rolls.

* deceased
[1] Correspondence and reprints; e-mail: Busse@uni-bayreuth.de

In this paper some of these questions are addressed and new dynamical features of finite amplitude convection at low values of P are pointed out. In view of the large parameter space a comprehensive description of all physically realizable forms of convection as a function of the Rayleigh number R, the Prandtl number P and the rotation parameter Ω goes much beyond the scope of the paper and will not be attempted here. Because of the prevalence of spatio-temporal chaos large scale numerical simulations will be required in the future to enhance our understanding of low Prandtl number rotating convection.

In the following we first outline in Section 2 the mathematical formulation of the problem and the methods of solution. We then discuss steady subcritical two-dimensional solutions in Section 3 and two-dimensional oscillatory solutions in Section 4. Except for very low values of Ω the two-dimensional solutions are generally unstable and are replaced by three-dimensional solutions with a chaotic time dependence. Some examples of these will be shown in Section 5. In Section 6 we shall consider the influence of rotation on traveling convection waves and in Section 7 some concluding remarks will be added.

2. Mathematical formulation and numerical methods

We consider a horizontal fluid layer of height h between two parallel rigid plates kept at the temperatures T_1 and T_2. The lower plate is kept at the higher temperature T_2. The layer is rotating about a vertical axis with the angular velocity Ω_d, but the centrifugal force is assumed to be negligible in comparison with gravity such that the physical conditions of the layer are homogeneous in the horizontal dimensions. This assumption is usually quite well satisfied in experimental situations for the values of the dimensionless rotation parameter Ω considered in this paper (Heikes and Busse [16]; Zhong et al. [5]). Using h as length scale, h^2/κ as time scale, where κ is the thermal diffusivity, and $(T_2 - T_1)/R$ as scale for the temperature, we obtain dimensionless equations for the velocity vector $\boldsymbol{v}$ and for the deviation θ of the temperature from the distribution of the basic state of pure conduction,

$$\nabla^2\boldsymbol{v} + \boldsymbol{k}\theta - 2\Omega\boldsymbol{k}\times\boldsymbol{v} - \nabla\pi = \left(\boldsymbol{v}\cdot\nabla\boldsymbol{v} + \frac{\partial}{\partial t}\boldsymbol{v}\right)P^{-1}, \tag{1a}$$

$$\nabla\cdot\boldsymbol{v} = 0, \tag{1b}$$

$$\nabla^2\theta - R\boldsymbol{k}\cdot\boldsymbol{v} = \boldsymbol{v}\cdot\nabla\theta + \frac{\partial}{\partial t}\theta, \tag{1c}$$

where $\boldsymbol{k}$ is the unit vector in the vertical direction. The three dimensionless parameters of the problem are the Rayleigh number R, the Prandtl number P and the rotation parameter Ω which are defined by

$$R = \frac{\gamma(T_2 - T_1)gh^3}{\nu\kappa}, \qquad P = \frac{\nu}{\kappa}, \qquad \Omega = \frac{\Omega_d h^2}{\nu}, \tag{2}$$

where γ is the thermal expansivity, g is the acceleration of gravity and ν is the kinematic viscosity. We have assumed the Boussinesq approximation of the basic Navier–Stokes equations of motion in that all material properties are assumed to be constant except for the density, the temperature dependence of which is taken into account only in the gravity term.

In order to eliminate the constraint (1b) of continuity we use the following general representation of the solenoidal velocity field,

$$\boldsymbol{v} = \boldsymbol{U} + \nabla\times(\nabla\varphi\times\boldsymbol{k}) + \nabla\psi\times\boldsymbol{k} \equiv U_x\boldsymbol{i} + U_y\boldsymbol{j} + \boldsymbol{\delta}\varphi + \boldsymbol{\varepsilon}\psi, \tag{3}$$

where $\boldsymbol{U}$ represents the horizontally averaged velocity field and the fluctuating components are described in terms of the scalar functions φ and ψ. Without loosing generality it can be assumed that the horizontal average of the latter, indicated by a bar, vanishes, $\bar{\varphi} = \bar{\psi} = 0$. A mathematical proof of the general representation has been given by Schmitt and von Wahl [17].

Using a Cartesian system of coordinates with the z-axis in the vertical direction we write the conditions at the rigid boundaries in the form

$$\boldsymbol{U} = 0, \qquad \varphi = \frac{\partial}{\partial z}\varphi = \psi = \theta = 0 \quad \text{at } z = \pm\frac{1}{2}. \tag{4}$$

We obtain the equation for the scalar functions φ and ψ by taking the z-components of the (curl)^2 and of the curl of equation (1a),

$$\nabla^4\Delta_2\varphi - \Delta_2\theta - 2\Omega\frac{\partial}{\partial z}\Delta_2\psi = P^{-1}\left[\boldsymbol{\delta}\cdot(\boldsymbol{v}\cdot\nabla\boldsymbol{v}) + \left(\frac{\partial}{\partial t} + \boldsymbol{U}\cdot\nabla\right)\nabla^2\Delta_2\varphi - \boldsymbol{U}''\cdot\nabla\Delta_2\varphi\right], \tag{5a}$$

$$\nabla^2\Delta_2\psi + 2\Omega\frac{\partial}{\partial z}\Delta_2\varphi = P^{-1}\left[\boldsymbol{\varepsilon}\cdot(\boldsymbol{v}\cdot\nabla\boldsymbol{v}) + \left(\frac{\partial}{\partial t} + \boldsymbol{U}\cdot\nabla\right)\Delta_2\psi - \boldsymbol{U}'\cdot\boldsymbol{\varepsilon}\Delta_2\varphi\right], \tag{5b}$$

where Δ_2 denotes the two-dimensional Laplacian, $\partial^2/\partial x^2 + \partial^2/\partial y^2$ and where $\boldsymbol{U}'$ denotes the z-derivative of $\boldsymbol{U}$. In addition, the equation for the mean flow $\boldsymbol{U}$ must be solved.

$$\left(\frac{\partial}{\partial t} - \frac{\partial^2}{\partial z^2}\right)\boldsymbol{U} + 2\Omega\boldsymbol{k}\times\boldsymbol{U} = \frac{\partial}{\partial z}\overline{\left(\Delta_2\varphi\left(\boldsymbol{\varepsilon}\psi + \nabla_2\frac{\partial}{\partial z}\varphi\right)\right)}, \tag{5c}$$

where ∇_2 denotes the vector operator $(\partial/\partial x, \partial/\partial y, 0)$.

We are solving equations (5) together with equation (1c) using the Galerkin method. For this purpose we expand the variables $\varphi, \psi, \theta, U_x, U_y$ into complete systems of functions satisfying the boundary conditions (4)

$$\varphi = \sum_{l,m,n} a_{lmn}\exp\{il\alpha_x x + im\alpha_y y\} f_n(z), \tag{6a}$$

$$\psi = \sum_{l,m,n} c_{lmn}\exp\{il\alpha_x x + im\alpha_y y\}\sin n\pi\left(z + \frac{1}{2}\right), \tag{6b}$$

$$\theta = \sum_{l,m,n} b_{lmn}\exp\{il\alpha_x x + im\alpha_y y\}\sin n\pi\left(z + \frac{1}{2}\right), \tag{6c}$$

$$U_x = \sum_n U_n \sin n\pi\left(z + \frac{1}{2}\right), \tag{6d}$$

$$U_y = \sum_n V_n \sin n\pi\left(z + \frac{1}{2}\right), \tag{6e}$$

where $f_n(z)$ denote the Chandrasekhar [11] functions which are defined by

$$f_n(z) = \begin{cases} \dfrac{\cosh\lambda_n z}{\cosh\lambda_n\frac{1}{2}} - \dfrac{\cos\lambda_n z}{\cos\lambda_n\frac{1}{2}} & \text{with } \tanh\lambda_n\frac{1}{2} = -\tan\lambda_n\frac{1}{2} \text{ for odd } n, \\ \dfrac{\sinh\lambda_n z}{\sinh\lambda_n\frac{1}{2}} - \dfrac{\sin\lambda_n z}{\sin\lambda_n\frac{1}{2}} & \text{with } \operatorname{cth}\lambda_n\frac{1}{2} = \cot\lambda_n\frac{1}{2} \text{ for even } n. \end{cases} \tag{7}$$

Most of the numerical work will be focused on the two-dimensional case for which the x-dependence of expressions (6) can be dropped. However in Section 5 we shall extend the numerical analysis for the description of three-dimensional convection.

After expressions (6) have been introduced into equations (5) and (1c) and the equations have been projected onto the system of expansion functions used in the representations (6) a system of nonlinear ordinary differential equations in time for the coefficients $a_{lmn}(t)$, $b_{lmn}(t)$, $c_{lmn}(t)$, $U_n(t)$, $V_n(t)$ is obtained. This system of equations can be solved through forward integrations in time after a truncation scheme has been introduced. We shall neglect all coefficients and corresponding equations satisfying

$$l + m + nf > N_T, \tag{8}$$

where f is usually set equal to unity and where N_T is the truncation parameter which can be increased until the physical properties of the solutions no longer change in a significant way. In the case of two-dimensional solutions with $l = 0$ values of N_T up to 22 have been used in the course of the present analysis. In cases when the horizontal periodicity interval is relatively large, corresponding to values of α_x and α_y less than 2, $f = 2$ is chosen in order to emphasize the horizontal resolution.

An important class of solutions described by expressions (6) is steady convection flows for which the coefficients $a_{lmn}, b_{lmn}, c_{lmn}$ are constant in time and the coefficients U_n and V_n vanish. In this case it is convenient to employ a Newton–Raphson iteration method for the determination of the unknown coefficients $a_{lmn}, b_{lmn}, c_{lmn}$. This procedure offers the advantage that unstable branches of steady solutions can also be determined. In the case of two-dimensional solutions we can drop all coefficients with $l \neq 0$ and employ further symmetries, if we restrict our attention to the type of solutions corresponding to the critical conditions as defined by linear theory,

$$a_{0-mn} = a_{0mn}, \qquad b_{0-mn} = b_{0mn}, \qquad c_{0-mn} = c_{0mn}, \tag{9a}$$

$$a_{0mn} = b_{0mn} = 0 \quad \text{for odd } m+n, \qquad c_{0mn} = 0 \quad \text{for even } m+n. \tag{9b}$$

The stability of steady two-dimensional solutions can be investigated through the superposition of arbitrary infinitesimal three-dimensional disturbances of the form

$$\tilde{\varphi} = \exp\{iby + idx + \sigma t\} \sum_{m,n} \tilde{a}_{mn} \exp\{im\alpha_y y\} f_n(z), \tag{10a}$$

$$\tilde{\psi} = \exp\{iby + idx + \sigma t\} \sum_{m,n} \tilde{c}_{mn} \exp\{im\alpha_y y\} \sin n\pi \left(z + \frac{1}{2}\right), \tag{10b}$$

$$\tilde{\theta} = \exp\{iby + idx + \sigma t\} \sum_{m,n} \tilde{b}_{mn} \exp\{im\alpha_y y\} \sin n\pi \left(z + \frac{1}{2}\right). \tag{10c}$$

After these expressions have been introduced into the linearized equations for the disturbances of a given steady two-dimensional solution characterized by the parameters R, Ω, P and α_y and the equations have been projected onto the expansion functions, a linear, homogeneous system of algebraic equations for the coefficients $\tilde{a}_{mn}, \tilde{b}_{mn}, \tilde{c}_{mn}$ is obtained with the growth rate σ as eigenvalue. Whenever there exists as a function of b and d an eigenvalue σ with a positive real part σ_r, the steady solution is unstable. Otherwise it will be regarded as stable. In the stability analysis always the same truncation parameter N_T as for the steady solution will be used for the disturbances of the form (10).

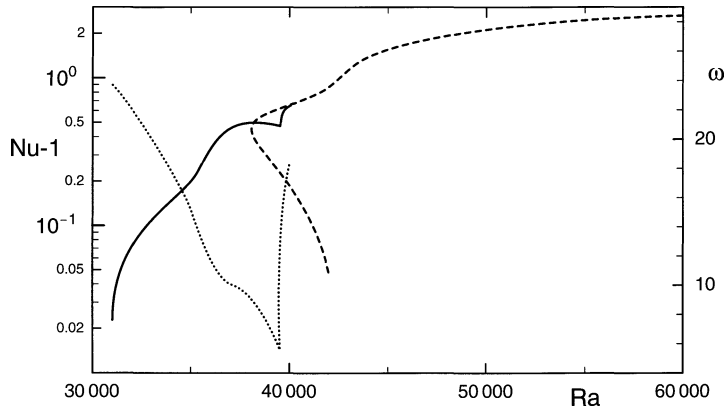

Figure 1. Nusselt number Nu of two-dimensional steady subcritical convection flow (dashed line) and of two-dimensional oscillatory convection flow (solid line) as function of the Rayleigh number R for the case $P = 0.2,\ \Omega = 300,\ \alpha_y = 6.4$. The dotted line describes the frequency ω of oscillation (right ordinate).

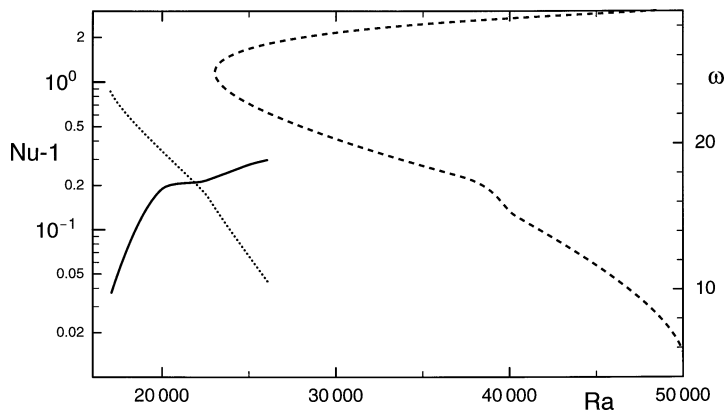

Figure 2. Same as *figure 1*, but for the case $P = 0.1,\ \Omega = 300,\ \alpha_y = 5.0$.

3. Subcritical steady two-dimensional convection

For the characterization of finite amplitude convection it is convenient to use the Nusselt number Nu which is defined as ratio of the heat transports in the presence and in the absence of convection. In *figures 1, 2* and *3* the Nusselt number has been plotted for steady subcritical convection in the form of two-dimensional rolls for various Prandtl numbers. Also shown are Nusselt numbers for oscillatory convection which will be discussed in Section 4. It is evident that the lower branch is characterized by rather low amplitudes of convection which decrease with decreasing Prandtl number, while the amplitude on the upper branch becomes relatively large with increasing values of R. The corresponding isotherms are shown in *figure 4* for some typical values of R. The increase of the Nusselt number is reflected in the formation of thermal boundary layers at the planes $z = \pm 1/2$. The same features are visible in the isotherms at a higher Prandtl number as shown in *figure 5*. Here also the component v_x of the velocity field parallel to the axis of the rolls has been plotted. It can be clearly seen that the character of this velocity changes from one described by $\sin\alpha_y y \sin 2\pi(z + 1/2)$ to one described by $\sin 2\alpha_y y \sin \pi(z + 1/2)$ as the principal mode. In this latter form the vertical component of vorticity of the x-component v_x of the velocity field exhibits a sign opposite to the global vorticity 2Ω at the places where v_y

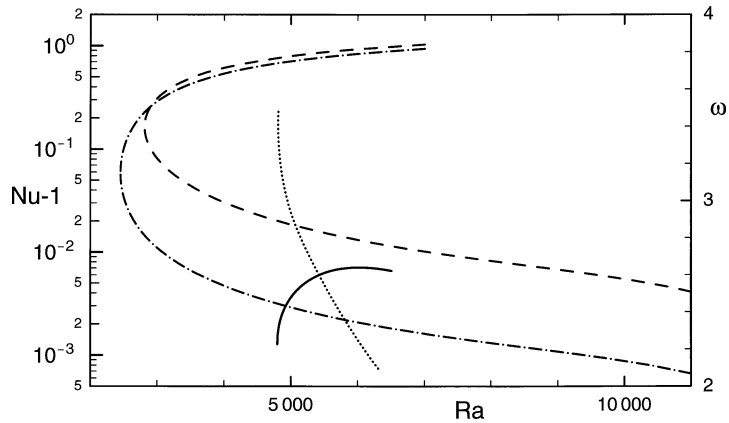

Figure 3. Same as *figure 1*, but for the case $P = 0.025,\ \Omega = 100,\ \alpha_y = 3.0$. Also shown is the Nusselt number Nu of two-dimensional steady convection in the case $P = 0.01,\ \Omega = 100,\ \alpha_y = 3.0$ (dash-dotted line).

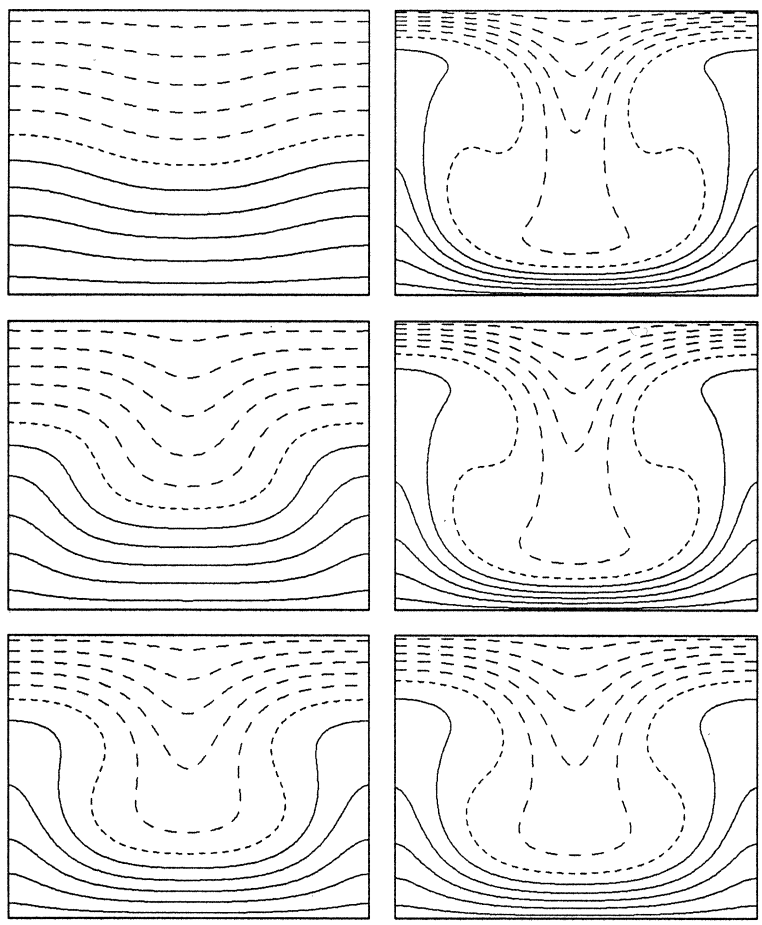

Figure 4. Isotherms in the $y-z$-plane of subcritical steady convection rolls in the case $P = 0.1,\ \Omega = 300,\ \alpha_y = 5.0$. The Rayleigh numbers are (from top to bottom) $R = 4.8 \cdot 10^4, 3.6 \cdot 10^4, 2.4 \cdot 10^4$. The solutions on the lower (upper) branch are shown in the left (right) column. Solid (dashed) lines indicate positive (negative) values. The line of very short dashes indicates zero.

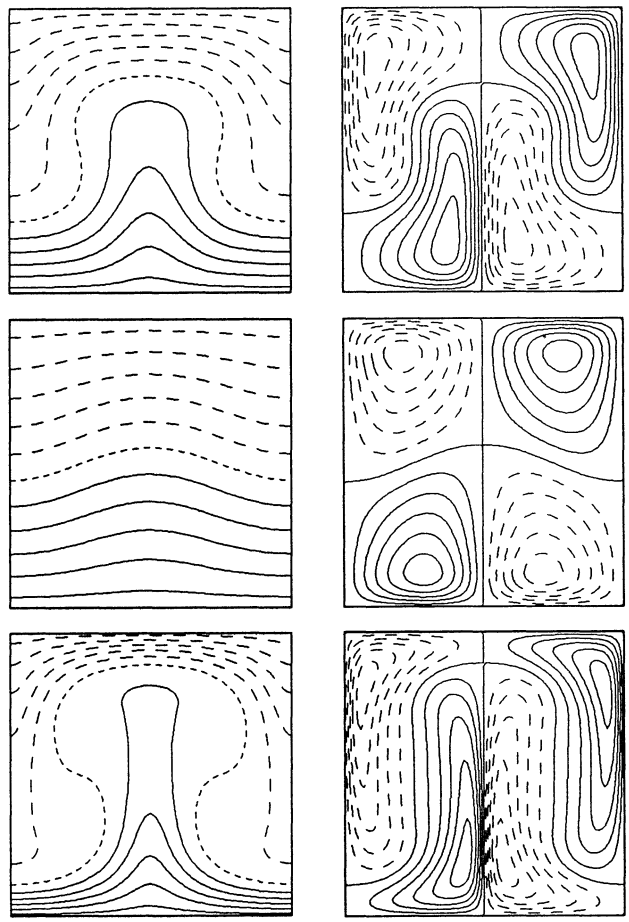

Figure 5. Isotherms (left column) and lines of constant velocity v_x (right column) are shown (from top to bottom) for $R = 4.8 \cdot 10^4$ (upper branch), $R = 4.8 \cdot 10^4$ (lower branch) and $R = 6 \cdot 10^4$ (upper branch) in the case $P = 0.2,\ \Omega = 300,\ \alpha = 6.4$.

reaches maximal absolute values. In this way the convection flow at finite amplitudes manages to counteract the constraining effects of rotation.

The wavenumbers α_y of the steady solutions discussed so far have been selected to nearly match the critical values of the wavenumber in the case of onset of oscillatory convection. When other wavenumbers are considered it becomes evident that steady solutions exist for even lower values of R. In *figures 6(a)* and *6(b)* the entire intervals of wavenumbers for which subcritical convection rolls exist are shown for selected values of the Rayleigh number. It can be seen that the subcritical range of the convection rolls becomes most extended for a wavenumber somewhat below the critical value. Even though the wavenumber chosen for the steady subcritical roll solution does not correspond to the value for which the minimum Rayleigh number can be reached, it is remarkable to notice that steady rolls exist far below the onset of oscillatory convection and almost down to the Rayleigh number for onset of convection in a non-rotating layer, if P is sufficiently small.

When the stability of the steady rolls is investigated with respect to disturbances of the form (10) in the special case $d = b = 0$, i.e. in the case when the horizontal periodicity interval of the rolls is not changed, the usual properties of a subcritical bifurcation are found. The lower branch is always unstable with respect to a monotonously growing mode while the upper branch is stable with respect to this special disturbance. In the

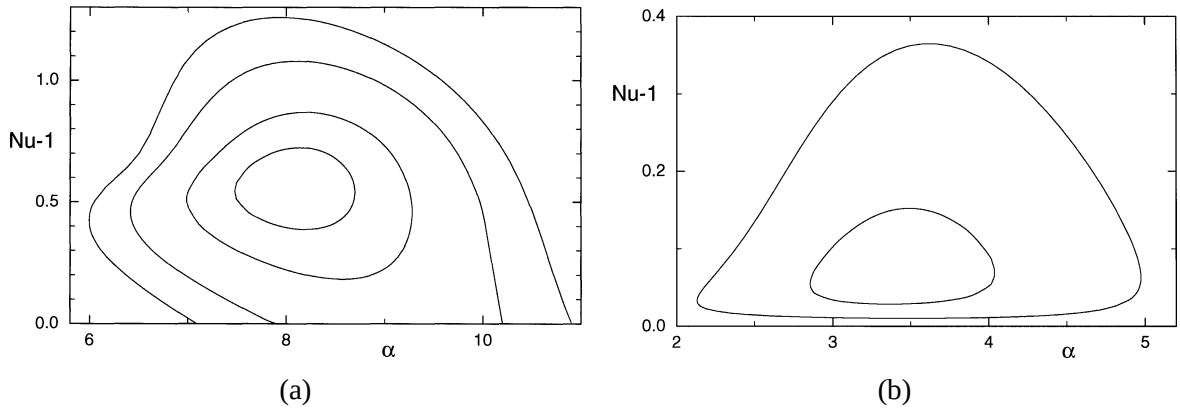

Figure 6. The Nusselt number Nu for steady convection rolls as function of the wavenumber α for (a) $R = 3.5 \cdot 10^4$ (innermost closed curve), $R = 3.6 \cdot 10^4$ (second closed curve), $R = 3.8 \cdot 10^4$ (next curve), and $R = 4 \cdot 10^4$ (outermost curve) in the case $P = 0.2,\ \Omega = 300$; for (b) $R = 3000$ (outer curve) and $R = 2500$ (inner curve) in the case $P = 0.01,\ \Omega = 100$.

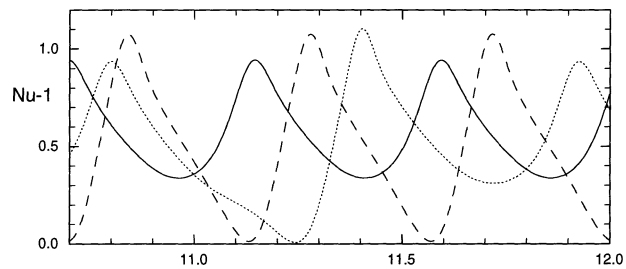

Figure 7. Nusselt number Nu as a function of time for two-dimensional oscillatory convection for $R = 3.9 \cdot 10^4$ (dashed curve), $R = 3.95 \cdot 10^4$ (dotted curve) and $R = 3.96 \cdot 10^4$ (solid curve) in the case $P = 0.2,\ \Omega = 300,\ \alpha_y = 6.4$.

case $P = 0.2$ part of the upper branch up to $R = 40000$ is unstable with respect to oscillatory disturbances. We shall return to this property in the next section.

4. Two-dimensional oscillatory convection

The onset of convection in the form of oscillations is a characteristic feature of a rotating low-Prandtl-number convection layer. The oscillations can assume the form of either traveling waves or standing oscillations if we restrict the attention to the two-dimensional case. Time integrations for two-dimensional convection for Rayleigh numbers above the critical value for the onset of oscillations have been carried out for $P = 0.2, 0.1,$ and 0.025. In all cases it was found that the time dependence evolves into standing oscillations in agreement with the theory of Clune and Knobloch [12] for the respective parameter values. For the standing oscillations the same symmetries (9) as for the steady solutions apply. The time-averaged Nusselt numbers of oscillatory convection are shown in *figures 1, 2* and *3* where also the variation in the frequency of oscillations can be seen. Typically the period of oscillation increases with the Rayleigh number. There is no indication that the period tends to infinity as the upper or lower branch of the steady solution is approached as must be expected if the oscillatory branch directly joins the steady branch. Instead the oscillatory convection changes its character in various ways. In the case $P = 0.2$ the period doubles as R reaches a values slightly below 39500 as shown in *figure 7*. While the sign of motion always reverses twice during each period of the normal standing oscillations,

the doubled period is a result of the property that one half of the reversals have disappeared. At $R = 39600$ a reversal of motion does no longer occur at all and the oscillations become superimposed onto a steady state of motion. In the case of reversing motion the Nusselt number period actually corresponds to the half period of oscillation because of the symmetry of the motions of both signs with respect to the midplane of the layer. This property is apparent from *figure 8* where the simple oscillation and the period-doubled oscillation are visualized through time sequences of isotherm plots. Only slightly more than half a period of oscillation is visualized in *figures 8(a)* and *8(b)* since the plots for the second half period can be derived from those of the first half period by a reflection of the isotherms with respect to the line $z = 0$ and by changing solid (dashed) lines to dashed (solid) lines. Beyond about $R = 39600$ the motion of rolls oscillates about a steady mean value and the average Nusselt number increases sharply while the amplitude of the oscillations decreases until the oscillatory branch meets the upper steady branch slightly above $R = 40000$ at a point of bifurcation. In contrast to the Takens–Bogdanov point found in a simple model of low Prandtl number rotating convection (Guckenheimer and Knobloch [18]) this bifurcation is a Hopf bifurcation. For this latter oscillation the period decreases with increasing R in contrast to the standing oscillations as is apparent from *figure 1*.

In the case $P = 0.025$ which corresponds to mercury as convecting liquid a period doubling sequence can be observed as shown in *figure 9*. By the time the Rayleigh number has reached 3400 the time dependence has become chaotic. Undoubtedly there will be windows where periodic oscillations can be obtained for $R > 3400$. But no special numerical effort has been made to investigate such states in detail. Neither in this case nor in the case of $P = 0.1$ has a connection been found between oscillatory convection and a Hopf bifurcation on the upper branch of steady two-dimensional convection as shown in *figure 1*.

5. Three-dimensional convection

Since all steady two-dimensional solutions are unstable with respect to the Küppers–Lortz instability as soon as Ω exceeds a critical value Ω_c of the order 10 which actually decreases with P, there can be little doubt that the subcritical steady two-dimensional solutions are also unstable on their upper branches with respect to three-dimensional disturbances. A general stability analysis has not been carried out because of the numerous parameters that are involved. Instead forward integrations in time based on the three-dimensional Galerkin representation have been done, motivated in part by experimental observation of subcritical convection by Bajaj and Ahlers [19]. In *figure 10* a typical result is shown for a horizontal periodicity interval $0 \leqslant x, y \leqslant 5 \cdot \pi/3$. The truncation parameter $N_T = 22$ with $f = 2$ has been used in the computations. However, the results show rather small differences if $N_T = 20$ is used for comparisons. The time sequence of plots shows that the rolls become unstable to a wavy instability, but then the distortions of the rolls decay, such that the rolls become nearly straight again until a new wavy distortion grows. This process resembles what has been observed in experiments. For slightly different parameter values the time dependence corresponds more closely to the Küppers–Lortz process in that rolls become unstable and are replaced by rolls oriented at an angle with respect to the original rolls. In the case of *figure 11* this angle is 90°. However, if a large periodicity interval had been chosen, a somewhat smaller angle could have been realized.

6. Obliquely traveling convection waves

Oscillatory convection in the form of ondulations traveling along the axis of the convection rolls is a typical phenomenon of convective motions in low Prandtl number fluids. The transition to oscillatory convection has been analyzed by Busse [20] and by Clever and Busse [21] and the finite amplitude properties have been studied

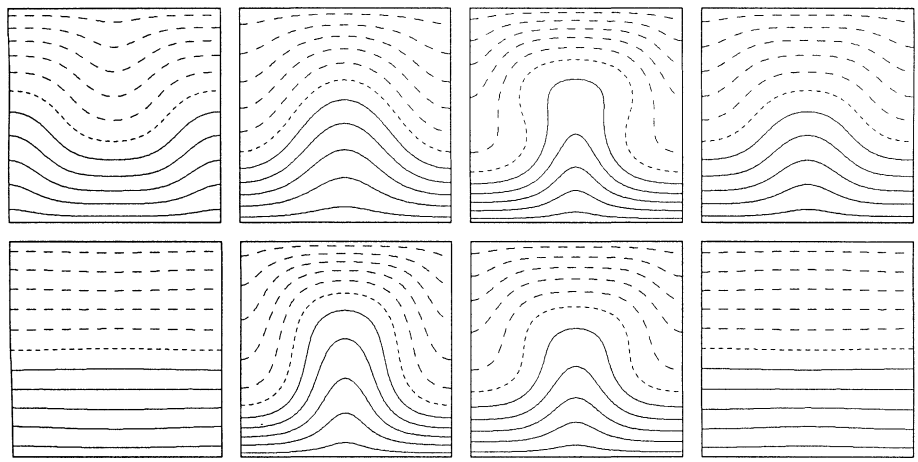

(a)

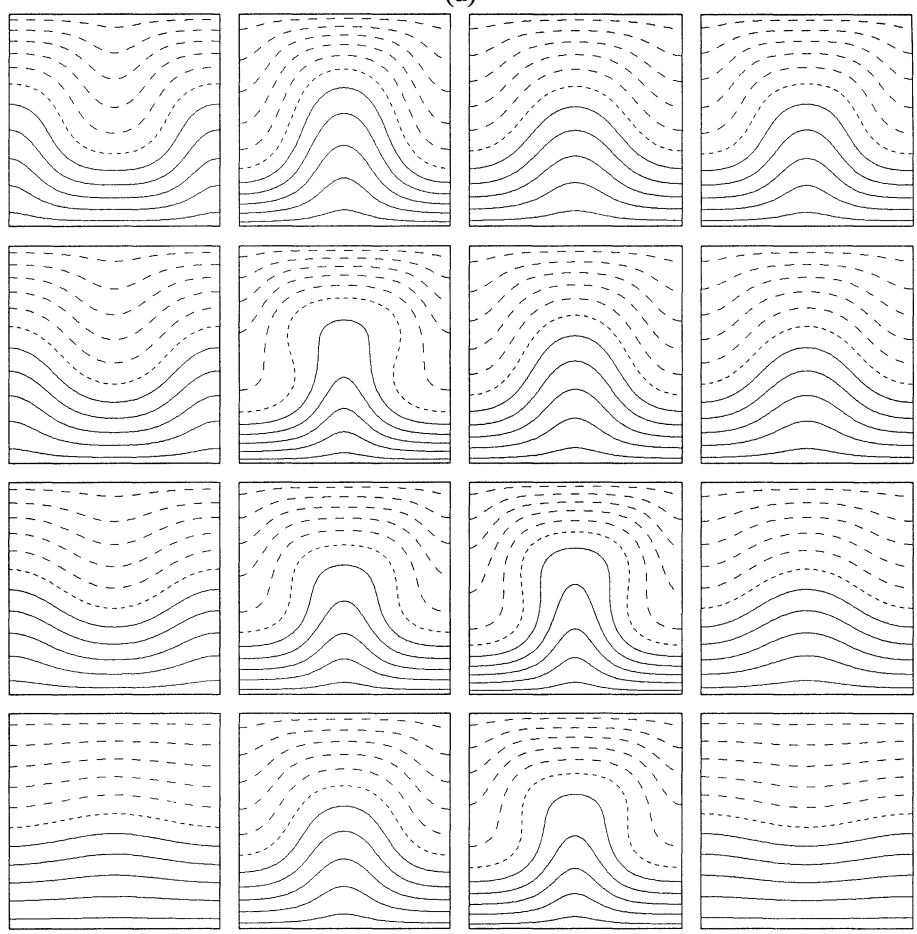

(b)

Figure 8. Isotherms of two-dimensional oscillatory convection in the case (a) $R = 3.8 \cdot 10^4$, $P = 0.2$, $T = 300$, $\alpha_y = 6.4$. The upper row shows plots at the times $t = n\pi/6\omega$ with $\omega = 9.211$, $n = 0, 1, \ldots, 7$ (from top to bottom, then left to right); (b) $R = 3.95 \cdot 10^4$. Plots are shown at the times $t = n\pi/12\omega$, with $\omega = 2.789$, $n = 0, 1, \ldots, 15$ (from top to bottom, then left to right).

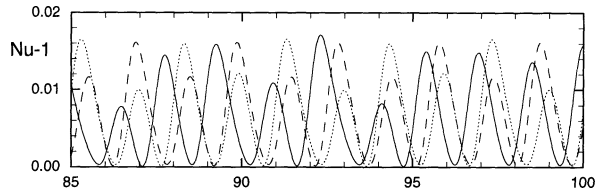

Figure 9. Nusselt number Nu as a function of time for the Rayleigh number $R = 6250$ (dotted), $R = 6320$ (dashed) and $R = 6400$ (solid) in the case $P = 0.025,\ \Omega = 100,\ \alpha_y = 3.0$.

in later papers of Clever and Busse [22–24]. The waves are often seen in experiments with air as convecting fluid (Willis and Deardorff [25]; Croquette and Williams [26]; Cakmur et al. [27]) and have also been found in numerical simulations (Lipps [28]; McLaughlin and Orszag [29]; Grötzbach [30]). Here we wish to draw attention to the property that these waves travel obliquely as soon as the convection layer rotates about a vertical axis and that their appearance is slightly skewed.

The latter property is just a consequence of the loss of the reflection symmetry about planes $x = \text{const.}$ in the rotating system. While the growing oscillatory disturbance in the non-rotating layer assumes the form

$$\tilde{\varphi} = \exp\{i\alpha_x x + i\omega t\}\varphi_0(y, z), \tag{11}$$

where $\varphi_0(y, z)$ is periodic in y with the same wavenumber α_y as the steady roll solution, the corresponding expression in a rotating layer is

$$\tilde{\varphi} = \exp\{i\alpha_x x + idy + i\omega t\}\varphi_0(y, z) \tag{12}$$

with a small, but finite value of d. This finite value of d has not been taken into account in the computations of the oscillatory instability by Clever and Busse [15]. But the curve for the onset of the latter instability shown in *figure 12* of that paper is not changed within the line width of the curve when finite values of d are taken into account. Because of the smallness of d, the skewness of the ondulations of the oscillating convection will not easily be seen in experiments and we draw attention to this effect only because of its principal nature.

The property of obliquely traveling convection waves in a rotating layer is a more striking phenomenon and it is independent of the finite value of d. At finite amplitudes an ondulatory wave traveling in the x-direction along the rolls is associated with a mean flow U_x which grows in proportion to the square of the amplitude of the wave (Clever and Busse [23]). In a rotating system this mean flow acquires a y-component perpendicular to the axis of the rolls owing to the action of the Coriolis force. As a consequence the entire pattern of rolls with superimposed wavy distortions drifts in y- as well as in the x-direction as shown in *figure 12*. In other words, the direction of the mean flow vector averaged over the layer height is turned opposite to the sense of rotation away from the roll axis by an angle γ. For small values of Ω the angle γ increases linearly with Ω. The computations for *figure 12* have been carried out for $d = 0$. Because of the smallness of d for the strongest growing oscillatory disturbance it is not feasible to do the computations with a suitably large horizontal periodicity interval. While the value $P = 1$ for which the computations have been performed is not really a low Prandtl number, we have used it as a representative value because experimental observations in layers of gases under higher pressure offer the best chance to observe the oscillatory instability.

7. Concluding remarks

The analysis of the preceding sections has exhibited some typical properties that characterize convection in rotating layers of low Prandtl number fluids. Since most of the computations have been restricted to two-

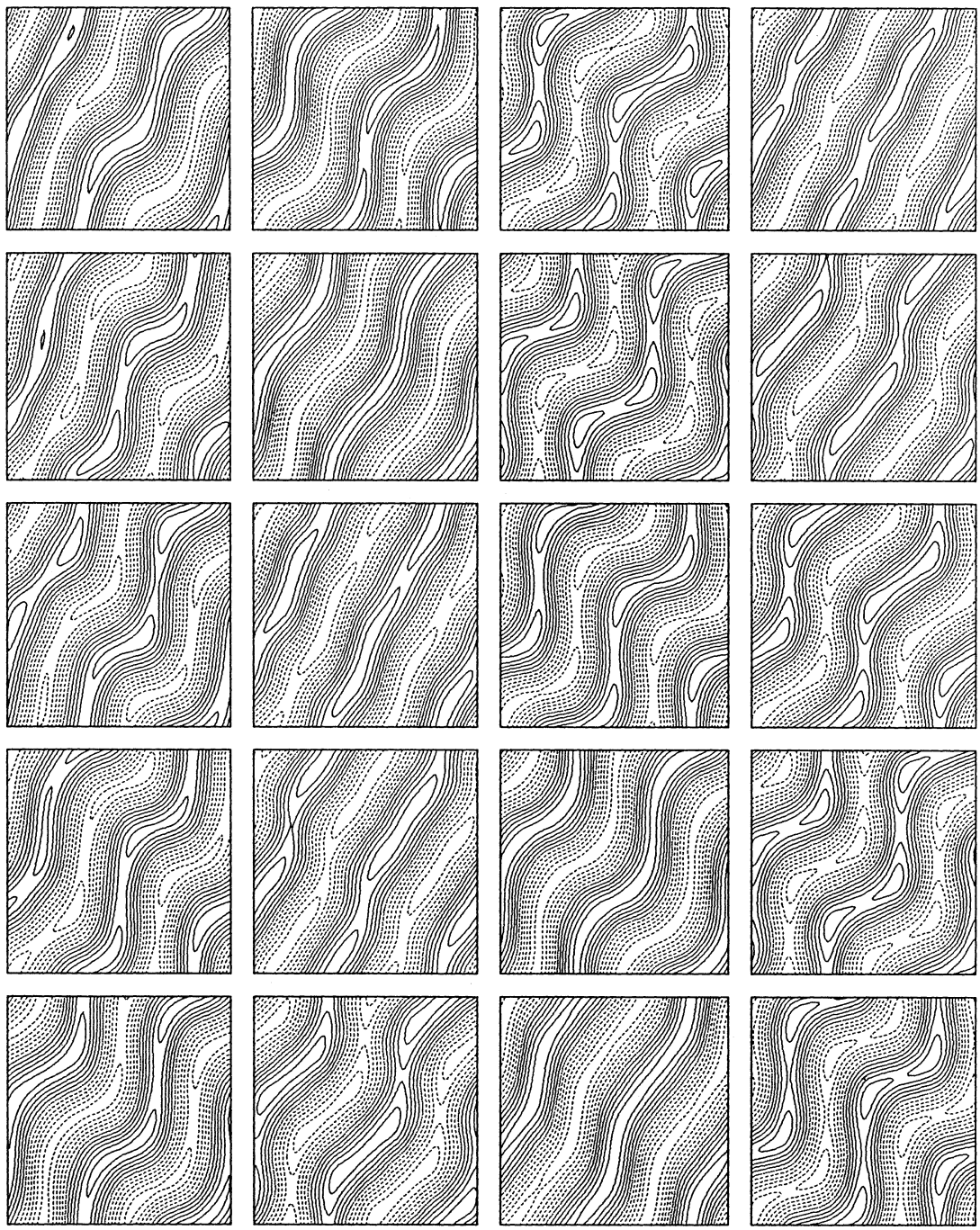

Figure 10. Time sequence (from top to bottom, first column, then second column) of plots of isotherms in the plane $z = 0$ at equidistant times ($\Delta t = 0.3$) for $P = 0.2,\ R = 5000,\ \Omega = 30,\ \alpha_x = \alpha_y = 1.2$.

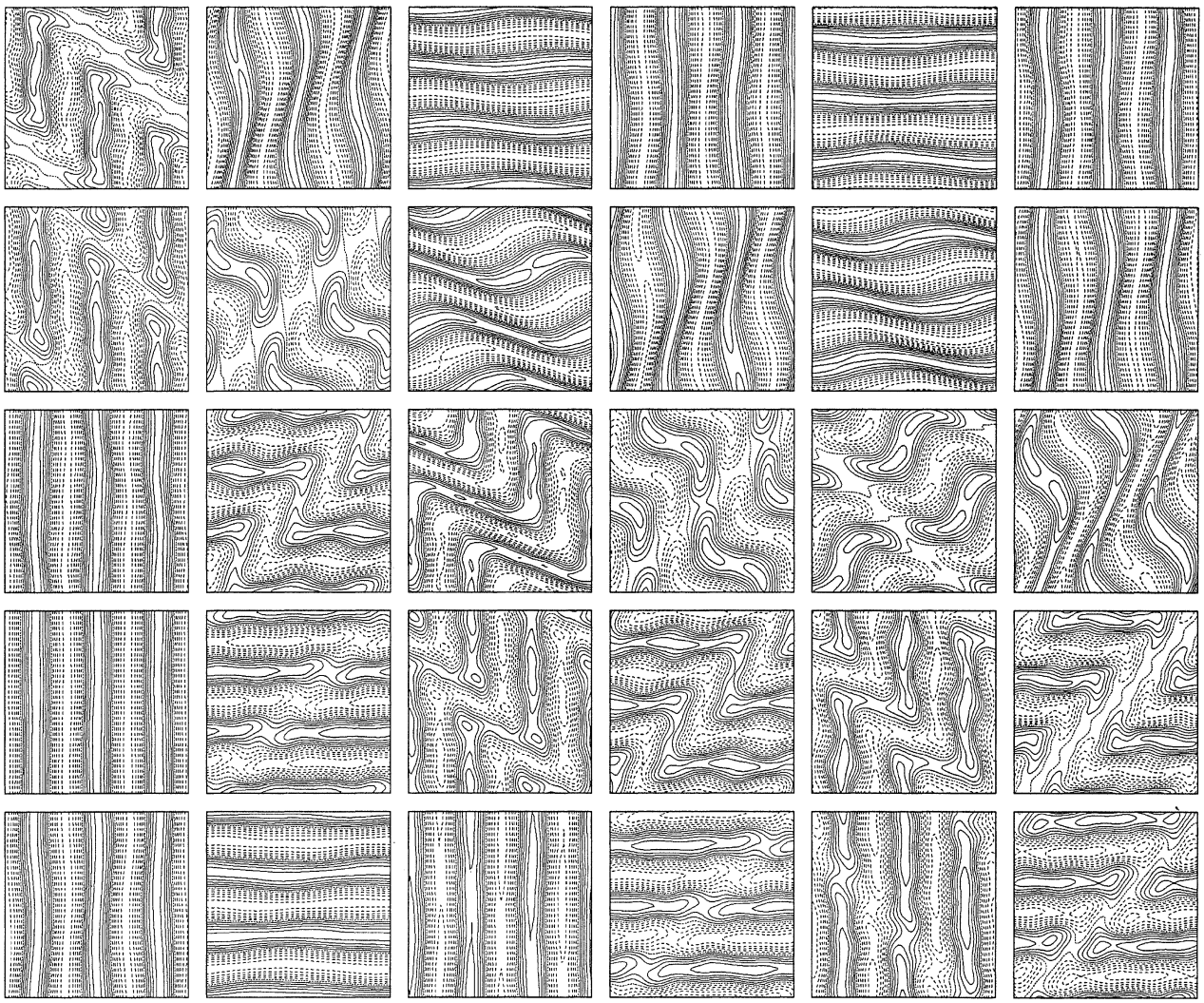

Figure 11. Same as *figure 10*, but for $P = 0.3,\ R = 6000,\ \Omega = 50,\ \alpha_x = \alpha_y = 1.5$.

dimensional convection flows which are unstable to three-dimensional disturbances, little correspondence to laboratory observations can be expected in this case. If, however, a uniform magnetic field $\boldsymbol{B}$ permeates the layer of an electrically conducting fluid, the two-dimensional roll-like flow aligned with $\boldsymbol{B}$ will be stabilized with respect to three-dimensional disturbances. As long as the flow does not depend on the coordinate in the direction of $\boldsymbol{B}$, the magnetic field does not enter the equations (5) for the two-dimensional case. Only when the Lorentz force exceeds the Coriolis force will convection rolls oriented obliquely with respect to the magnetic field become preferred (Eltayeb [31]). It thus appears to be possible to design experiments where the processes discussed in Sections 3 and 4 can be observed. Alternatively narrow channels could be used to enforce approximate two-dimensionality of convection.

The ongoing experiments by Bajaj and Ahlers [19] so far have shown only the three-dimensional kind of convection described in Section 5. But since their shadowgraph visualization of convection in compressed gases allows them to reach $P = 0.17$ there does exist the possibility that oscillatory convection could eventually be observed.

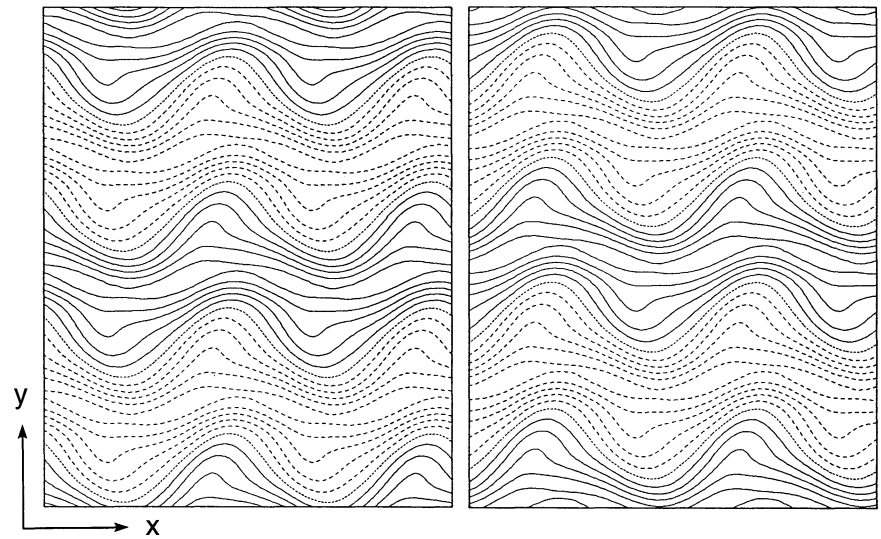

Figure 12. Lines of constant vertical velocity in the plane $z = 0$ in the case $\Omega = 5$, $R = 8000$, $P = 1.0$ with $\alpha_x = 2.2$, $\alpha_y = 1.8$ at the times $t = 0$ (left) and $t = 0.135$ (right), i.e. approximately half a period later.

The results of this paper emphasize the important role played by the Prandtl number in the properties of finite amplitude convection in a rotating fluid layer. In numerical studies of high Prandtl number convection in rotating systems usually the case $P = 1$ is assumed for simplicity (see, for example, Julien et al. [10], and references therein). However, significant changes in the properties of turbulent convection must be expected when the Prandtl number is much less than one as in liquid metals or in dense plasmas where radiative heat transfer keeps the thermal diffusivity high. For a study of the P-dependence of convection in rotation spherical shells we refer to the recent paper of Tilgner and Busse [32].

References

[1] Goldstein H.F., Knobloch E., Mercader I., Net M., Convection in a rotating cylinder I: Linear theory for moderate Prandtl numbers, J. Fluid Mech. 248 (1993) 583–604.
[2] Herrmann J., Busse F.H., Asymptotic theory of wall-attached convection in a rotating fluid layer, J. Fluid Mech. 255 (1993) 183–194.
[3] Kuo E.Y., Cross M.C., Traveling-wave wall states in rotating Rayleigh–Bénard convection, Phys. Rev. E 47 (1993) 2245–2248.
[4] Busse F.H., Heikes K.E., Convection in a rotating layer: A simple case of turbulence, Science 208 (1980) 173–175.
[5] Zhong F., Ecke R., Steinberg V., Rotating Rayleigh–Bénard convection: Küppers–Lortz transition, Physica D 51 (1991) 596–607.
[6] Hu Y., Ecke R.E., Ahlers G., Time and length scales in rotating Rayleigh–Bénard convection, Phys. Rev. Lett. 74 (1995) 5040–5043.
[7] Tu Y., Cross M.C., Chaotic domain structure in rotating convection, Phys. Rev. Lett. 69 (1992) 2515–2518.
[8] Millán-Rodriguez J., Bestehorn M., Pérez-Garcia C., Friedrich R., Neufeld M., Defect motion in rotating fluids, Phys. Rev. Lett. 74 (1995) 530–533.
[9] Pesch W., Complex spatio-temporal convection patterns, Chaos 6 (1996) 348–357.
[10] Julien K., Legg S., McWilliams J., Werne J., Rapidly rotating Rayleigh–Bénard convection, Phys. Rev. E 47 (1993) 2245–2248.
[11] Chandrasekhar S., Hydrodynamic and Hydromagnetic Stability, Clarendon Press, Oxford, 1961.
[12] Clune T., Knobloch E., Pattern selection in rotating convection with experimental boundary conditions, Phys. Rev. E 47 (1993) 2536–2550.
[13] Veronis G., Motions at subcritical values of the Rayleigh number in a rotating fluid, J. Fluid Mech. 24 (1966) 545–554.
[14] Veronis G., Large-amplitude Bénard convection in a rotating fluid, J. Fluid Mech. 31 (1968) 113–139.
[15] Clever R.M., Busse F.H., Nonlinear properties of convection rolls in a horizontal layer rotating about a vertical axis, J. Fluid Mech. 94 (1979) 609–627.
[16] Heikes K.E., Busse F.H., Weakly nonlinear turbulence in a rotating convection layer, Ann. NY Acad. Sci. 357 (1980) 28–36.
[17] Schmitt B.J., von Wahl W., Decomposition of solenoidal fields into poloidal fields, toroidal fields and the mean flow. Applications to the boussinesq-equations, in: Heywood J.G., Masuda K., Rautmann R., Solonnikov S.A. (Eds), The Navier–Stokes Equations II–Theory and Numerical Methods, Springer Lecture Notes in Math., Vol. 1530, 1992, pp. 291–305.

[18] Guckenheimer J., Knobloch E., Nonlinear convection in a rotating layer: amplitude expansions and normal forms, Geophys. Astro. Fluid Dyn. 23 (1983) 247–272.
[19] Bajaj K.M.S., Ahlers G., Rayleigh–Bénard convection with rotation at a Prandtl number of 0.17, B. Am. Phys. Soc. 43 (1998) 1999.
[20] Busse F.H., The oscillatory instability of convection rolls in a low Prandtl number fluid, J. Fluid Mech. 52 (1972) 97–112.
[21] Clever R.M., Busse F.H., Transition to time-dependent convection, J. Fluid Mech. 65 (1974) 625–645.
[22] Clever R.M., Busse F.H., Nonlinear oscillatory convection, J. Fluid Mech. 176 (1987) 403–417.
[23] Clever R.M., Busse F.H., Nonlinear oscillatory convection in the presence of a vertical magnetic field, J. Fluid Mech. 201 (1989) 507–523.
[24] Clever R.M., Busse F.H., Convection at very low Prandtl numbers, Phys. Fluids A2 (1990) 334–339.
[25] Willis G.E., Deardorff J.W., The oscillatory motions of Rayleigh convection, J. Fluid Mech. 44 (1970) 661–672.
[26] Croquette V., Williams H., Nonlinear competition between waves on convective rolls, Phys. Rev. A 39 (1989) 2765.
[27] Cakmur R.V., Egolf D.A., Plapp B.B., Bodenschatz E., Bistability and competition of spatiotemporal chaotic and fixed point attractors in Rayleigh–Bénard convection, Phys. Rev. Lett. 79 (1997) 1853–1856.
[28] Lipps F.B., Numerical simulation of three-dimensional Bénard convection in air, J. Fluid Mech. 75 (1976) 113–148.
[29] McLaughlin J.B., Orszag S.A., Transition from periodic to chaotic thermal convection, J. Fluid Mech. 122 (1982) 123–142.
[30] Grötzbach G., Direct numerical simulation of laminar and turbulent Bénard convection, J. Fluid Mech. 119 (1982) 27–53.
[31] Eltayeb I.A., Hydromagnetic convection in a rapidly rotating fluid layer, P. Roy. Soc. Lond. A 326 (1972) 229–254.
[32] Tilgner A., Busse F.H., Finite amplitude convection in rotating spherical fluid shells, J. Fluid Mech. 332 (1997) 359–376.